Evaluation of material profiles for III-V nanowire photodetectors

Cristina Martinez-Oliver[1], Kirsten E. Moselund[2], Vihar P. Georgiev[1]

Device Modelling Group, University of Glasgow, Glasgow G12 8QQ, United Kingdom[1]

IBM Research Europe, Säumerstrasse 4, 8803 Rüschlikon, Switzerland[2]

Abstract— **In this paper we report the simulation-based design of experiment (DoE) study for three different types of III-V based pin photodetectors operating at various wavelengths. Our DoE work shows that the optimal configuration for each device is strongly determined by the wavelength at which we are aiming to operate the photodetector and that a trade-off exists between low dark current and high photocurrent. Heterostructure devices provide the optimum performance in particular for longer wavelengths.**

INTRODUCTION

III-V materials are key to realising dense emitters for on-chip integrated photonics. Although group-IV based detectors are currently the state-of-the-art due to their ease of integration, when considering full optical links there is also a keen interest in using III-V materials for the photodetection, and in recent years there has been a lot of progress in this field [1,2]. IBM has demonstrated the monolithic integration of scaled InGaAs (50% In) photodetectors on Si [3], and are moving towards InP/InGaAS/InP heterostructure devices [4]. In the present work we evaluate by Technology Computer-Aided Design (TCAD) simulations the performance trade-off between different III-V material combinations. Notably homo-junction devices in InP and $In_{0.55}Ga_{0.45}As$ and a heterojunction device consisting of lattice matched combination of InGaAs sandwiched in between two InP layers.

All simulations are conducted using coupled 3D opto-electrical simulations with Sentaurus Electromagnetic Wave (EMW) Solver [5] for finite-difference time-domain (FDTD) calculations and Sentaurus Device [5] for electrical transport.

RESULTS AND DISCUSSION

Here we evaluate three devices based on a combination of two different materials: $In_{0.55}Ga_{0.45}As$ and InP. All devices have the same architecture and dimensions – comparable to the devices experimentally demonstrated by IBM. We use free-space detection as the purpose is to evaluate the impact of the material composition rather than an optimization of the device architecture or coupling schemes which might be highly wavelength dependent. This however also implies that we cannot properly evaluate the responsivity, but with the architecture used we compare the efficiency based on dark- and photo-current levels. The top part of Fig. 1 shows the simulation domain together with the device geometry and source of light. The nanowires' height is 220 nm and width is 200 nm. The p and n regions length is 375 nm and the i region is 250 nm. The oxide BOX below has a thickness of 500 nm, which would be sufficient to assure optical isolation in a fully integrated scheme. The bottom part of Fig. 1 presents the optical generation-coloured plots for each device. The excitation line is placed 500 nm above the nanowire and the metal contacts are considered to be transparent. This is done to avoid the impact of metal absorption and reflection when evaluating the wavelength dependence. On the optical generation plots it can be seen that the optical generation on the InP material areas reduces more rapidly in comparison to the $In_{0.55}Ga_{0.45}As$ region when increasing the excitation laser wavelength from 800 nm to 1300 nm. This is also expected as InP has a higher band-gap (1,27 eV) compared to $In_{0.55}Ga_{0.45}As$ (0,73 eV), see fig. 5, and therefore has a cut-off at 977 nm.

Fig. 2 shows the absorption response of the current for the three structures as a function of wavelength (λ). As expected, they all drop off gradually with increasing λ. InP provides efficient detection at the shorter λ, whereas it drops off rapidly close to its band-edge at 900-1000 nm. In both the homo-junction and the hetero-junction structure, the $In_{0.55}Ga_{0.45}As$ is the active absorption material so the absorption edge is pushed further into the NIR. The heterostructure nanowire reaches the peak current at $\lambda \sim 1000$ nm. The pure InGaAs device has its highest photocurrent at slightly longer wavelengths, most likely as a result of the larger volume of InGaAs.

In Fig. 3 the power sweep of signal power is shown for two different wavelengths, at a reverse bias of -0,5 V. The dotted lines correspond to the logarithmic scale of the plotted data. We observe a linear increase in all cases for 800nm, and a markedly lower efficiency at 1300nm, with the lowest being for the pure InP device, which correlates with the lower optical generation observed in Fig. 1.

In Fig. 4 we can see the current-voltage (I-V) curves at four different laser powers and two different wavelengths. Here, the benefit of the larger bandgap of InP is evident in a much lower dark current. For the heterostructure the InP barriers result in a dark-current in between the other two structures, while it reaches roughly the same photocurrent values as the pure InGaAs device.

Figure 5 shows the band diagrams for the three nanowire structures together with their electron and hole densities at -2 V of applied bias. As the heterostructure nanowire is made from two different materials, at the interface between the materials the band structure shows a step-like profile. This step explains the behaviour of the electrons and holes in the two plots below. The InP nanowire has its lowest density of electrons on the p side and of holes on the n side. Even though the p and n regions of the heterostructure are also made of InP, the number of electrons and holes remaining in those areas is higher. This is due to the energy barriers that both electrons and holes cannot surpass easily.

In conclusion, III-V material will provide for efficient scaled detectors for photonic integrated circuits (PIC) in the NIR. For shorter wavelengths of less than 900 nm all structures have very similar detection efficiency, and the large bandgap of InP provides an advantage in terms of very small dark current. However, at wavelengths beyond the Si absorption edge of main interest for PICs (here 1300 nm) the heterostructure device provides the best trade-off in terms of low dark current while achieving the same levels of

photocurrent as the pure InGaAs device. All of those results are in very good agreement with the underlying device physics and experimental results achieved so far.

ACKNOWLEDGEMENTS

REFERENCES

[1] A. Tosi, F. Acerbi, M. Anti, F. Zappa, "InGaAs/InP Single-Photon Avalanche Diode With Reduced Afterpulsing and Sharp Timing Response With 30 ps Tail," *IEEE Journ. of Quantum Electronics*, vol. 48, p. 1227, 2012.
[2] K. Chiba, A. Yoshida, K. Tomioka, J. Motohisa, "Vertical InGaAs Nanowire Array Photodiodes on Si," *ACS Photonics*, vol. 6, p. 260, 2019.
[3] S. Mauthe et al. "High-speed III-V nanowire photodetector monolithically integrated on Si," *Nature Communications*, vol. 11, p. 4565, 2020.
[4] P. Tiwari et al., accepted for OFC 2021, unpublished.
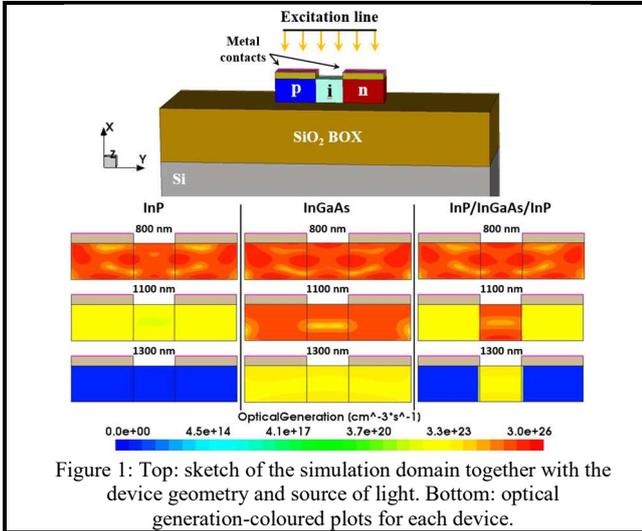[5] Sentaurus Device & EMW Solver, Version O-2018.06.

Figure 1: Top: sketch of the simulation domain together with the device geometry and source of light. Bottom: optical generation-coloured plots for each device.
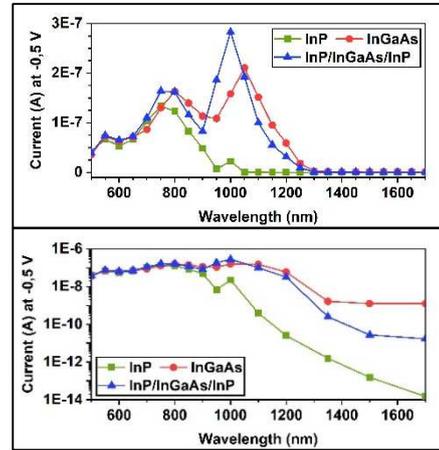

Figure 2: Current as a function of the wavelength for all devices at linear (top) and logarithmic (bottom) scale.
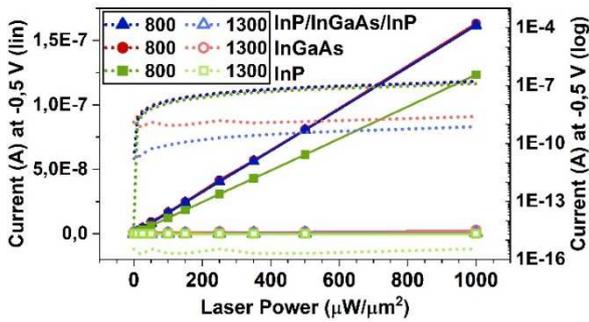

Figure 3: Current response in linear (solid lines with symbols) and logarithmic (dotted lines) scale for all devices as a function of the laser power.
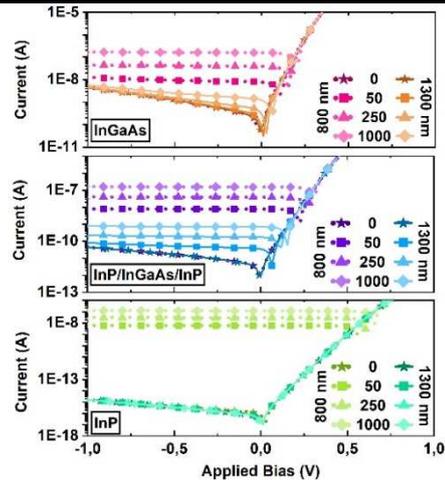

Figure 4: I-V curves for the three structures at four different laser powers (units of $\mu W/\mu m^2$) and two different wavelengths.
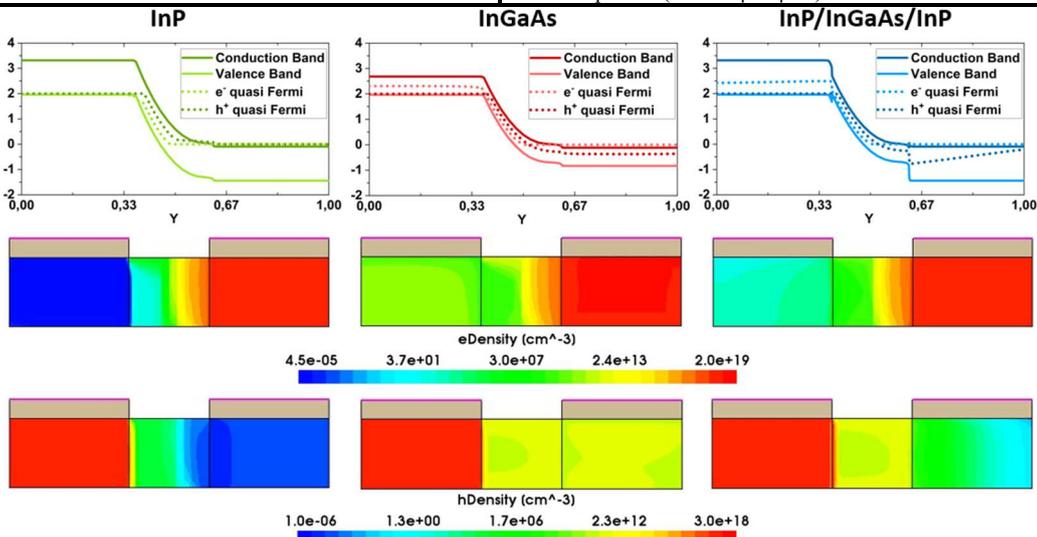

Figure 5: Top row: the band diagrams for the three nanowires along the length of the devices. Middle row is their electron density. Bottom row is the hole densities. All simulations are presented at -2 V of applied bias.